Impact Response of Tubular Structure with Internally Stacked Circular Rings

Naziratie Assrinie Assan, Amir Radzi Ab. Ghani, Ramzyzan Ramly
Faculty of Mechanical Engineering, Universiti Teknologi MARA, Shah Alam, Selangor.

ABSTRACT

During collision, occupants and structures experience serious injuries and damages due to high impulsive force and poor impact energy absorption. Performance of energy absorption can be improved by selecting a suitable structure and material. A good crashworthiness structure should have low Initial Peak Force (IPF), high Crush Force Efficiency (CFE) and high Specific Energy Absorption (SEA). This paper introduces a new design that consists of stacked circular tubes within a square column which will be subjected to axial impact loading. The impact results were compared to static analysis of previous study in terms of IPF, CFE, SEA and DAF. Simulation results were validated by experiment before on embarking simulation parametric study. The experiment was conducted using the Drop Hammer Machine, Instron Dynatup 8250. Simulation results show good agreement with the experimental results. The increase in IPF and SEA were influenced by inertia compared to static at the same crush distance. Critical parameters were determined to give the best crushing performance among stacked tubes designs. From this study, it can be concluded that the best crushing performance depends on the dominant structure, amount of plastic hinge and structure stiffness.

Keywords: *impact analysis, energy absorption, stacked tubes,*

Introduction

ISSN 1823- 5514, eISSN 2550-164X
Received for review: 2017-05-24
Accepted for publication: 2019-10-15
Published: 2019-12-31
© 2019 Faculty of Mechanical Engineering,
Universiti Teknologi MARA (UiTM), Malaysia.

Different types of energy absorbers are being studied in the quest for improving safety of vehicles and structures. Energy absorbers are mainly utilised in structures such as impact attenuator, personal safety equipment, packaging structure and drop cargo. Its purposes are to avoid severe injuries to occupants and reduce damages to structures by controlling the high initial impact force. For example, impact attenuator or crash box is used to control the impact force during collision by dissipating it in the safe manner instead of transferring it directly to occupants.

More than 1.2 million people were killed as a result of road traffic injuries as highlighted in 2015 global status report [1]. In the event of collision, they had experienced long term adverse health consequences due to serious head and brain injuries. According to A.A. Faieza and H. Shahul [2], proper design and material selection contribute to better impact energy absorption thus increasing safety of the occupants. This paper aims to study the crush response of aluminium square tube with internally stacked circular rings subjected to axial impact loading. The proposed configuration is expected to exhibit low impact force with high energy absorption.

Energy absorption

In the event of collision, kinetic energy is dissipated by the energy absorber through plastic deformations. Force-displacement curve is used to evaluate the crushing response of the design configuration. The ideal energy absorber demonstrates a long and flat force-displacement curve. An efficient energy absorber should be designed as such. Examples of structures used as energy absorbers are frusta [3], tubes with buckling initiator [4], windowed tubes [5], multi-cornered tubes [6], bi-structures tubes [7], multi-cell prismatic structures [8], corrugated tubes [9], patterned tubes [10] and honeycombs (shown in Figure 1) [11]. MA Yahaya et al. [12] carried out experimental study of aluminium honeycomb sandwich panels subjected to foam projectile impact and found out that it has good impact energy absorption.Performance of energy absorption can be measured by determining the specific energy absorption (SEA) as shown in equation (1). It can be calculated by dividing internal energy obtained through deformation by the mass of structure.

$$SEA = \frac{Internal\ Energy, IE\ (kJ)}{Mass, m\ (kg)} \quad (1)$$

High impulsive force acts on the structure during crash and it is transferred through the crumple zone and must not exceed the safety limit of the occupants. Worcester Polytechnic Institute (WPI's) developed an impact attenuator for its Formula SAE car to ensure driver safety in the event of crash [13]. Zhang X.W. et.al [4] introduced a buckling initiator to reduce the initial force which is usually high so that the effect of impact will be minimized. Upon deformation of constrained circular tubes, crush force

efficiency (CFE) can be maximized due to the presence of highly concentrated plastic hinge under lateral loading. CFE can be calculated by dividing the mean force in force-displacement curve by the initial peak force (IPF) (equation (2)) [14]. To determine the relationship between static and impact loading, dynamic amplification factor (DAF) is used to calculate the ratio of energy absorbed under impact to static loading (equation (3)).

(a)  (b) 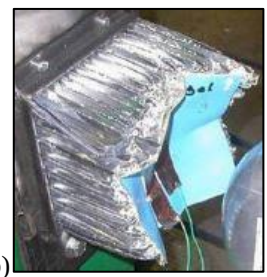

Figure 1: Deformation of honeycomb structure impacted by spherical indenter [11]

$$CFE = \frac{Mean\ Force\ (kN)}{Peak\ Force\ (kN)} \text{ x } 100\% \quad (2)$$

$$DAF = \frac{Impact\ energy\ Absorbed\ (kJ)}{Static\ energy\ absorbed\ (kJ)} \quad (3)$$

Design Model

Based on the axial crushing response of square tube and lateral crushing response of circular tube, a new structural configuration is proposed. A square tube subjected to axial loading exhibits high energy absorption but at the expense of high peak force. A circular tube under lateral loading shows lower energy absorption and lower peak force. Combining the two characteristics, it is hoped the best of both worlds can be achieved. The performance of proposed structure shall be quantified in terms of IPF, CFE and SEA. The structure is made from aluminium square and circular tubes, assembled into a specified configuration as shown in Figure 2.

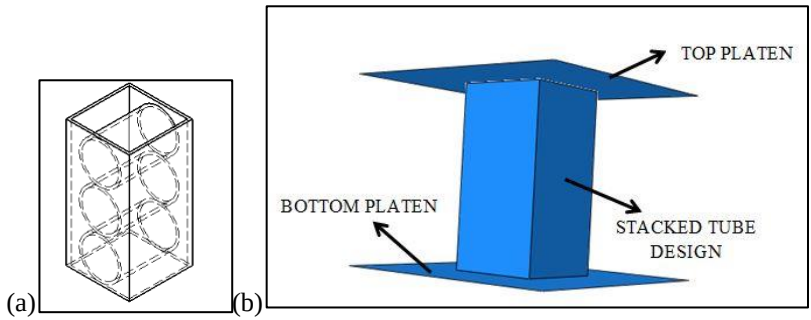

Figure 2: Isometric view of tubular structure internally stacked circular rings (a) hidden view of stacked tubes design, (b) shaded view

Finite Element Analysis

Finite element simulations are carried out using ABAQUS software. Simulation results are validated by experiments before embarking on simulation parametric study. In industrial practice, simulation is a vital procedure to ensure structure conformance to requirements so that cost of fabrication and time can be reduced [15].

In ABAQUS, the top and bottom platens are modelled as discrete rigid shell comprising of 8 discrete 4-noded quad elements. A reference point is assigned to the top platen to record the displacement and acceleration. A point mass of 24.54 kg is attached to this reference point. Impact velocity of 6 m/s is assigned to the top plate. Another reference point is assigned to the bottom platen to record the reaction force. The square and circular tubes are modelled as deformable shell. The circular tube is made up 2800 S4R quad elements while the square tube has 11781 S4R quad elements. A coefficient of friction of 0.25 is used for all contacting surfaces. Table 1 shows the material properties of Aluminium Alloy AA 6063-T5 obtained from ASTM E8 tensile test.

Table 1: Material properties of Aluminium Alloy AA6063-T5

Density	2700 kg/m3
Ultimate tensile strength (UTS)	220 Mpa
Yield strength	180 Mpa
Young's Modulus	65 Gpa
Poisson's Ratio	0.3
Plastic strain at UTS	0.1

Specimen fabrication

Figure 3 shows the dimension of the fabricated specimen. Square and circular aluminium tubes are cut into specified length using a band saw and finished using a lathe machine to ensure dimensional accuracy. A spirit level is used to ensure the top and bottom edges of the square tube are perpendicular to the tube axis. Fabricated components and assembled structure are shown in Figure 4.

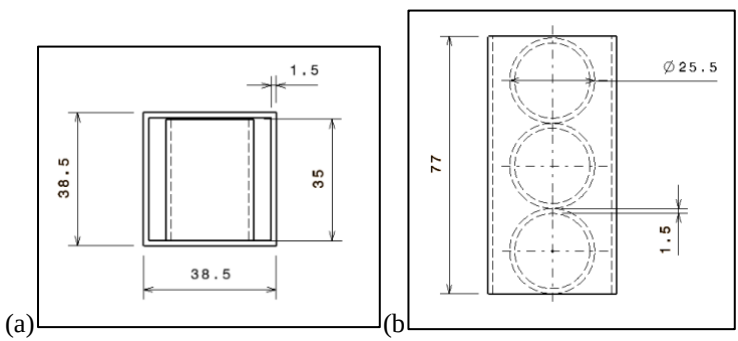

Figure 3: Dimension (in mm) of tubular structure with internally stacked circular rings ; (a) Top View, (b) Front View

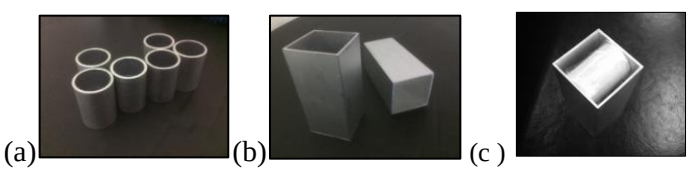

Figure 4: Fabricated components; a) circular tubes b) square tubes, and c) assembled structure

Experiment set up

Impact testing is conducted using an Instron Dynatup 8250 drop hammer machine. Figure 5 shows the experimental set up of the impact test. The machine is pneumatically assisted to enable higher drop hammer impact speed. The speed of the drop hammer is controlled by adjusting the drop height and compressor pressure. Steel plate with a mass of 24.54 kg is attached to the top platen and the impact speed is set at 6 m/s. The force, distance and acceleration are recorded by the accelerometer in the tup.

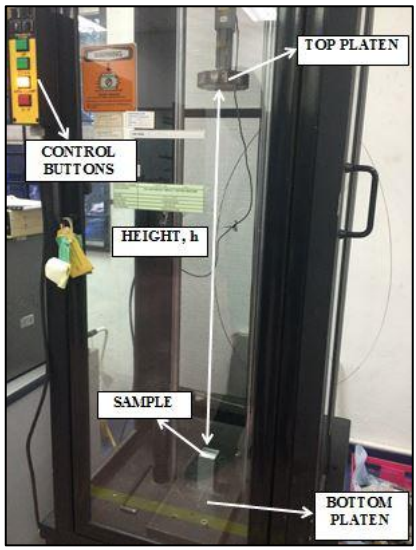

Figure 5: Impact testing machine used to run impact testing

Simulation of stacked tubes subjected to axial impact loading

Parametric study by simulation was carried out to determine the critical parameters that have significant effect on crush response of stacked tubes with different variations. They are classified into three groups based on the type of variation. The first group looks at the arrangement of tubes; S.A-1, S.A-2, S.A-3 and S.A-4. Large and small circular tubes were used in specimen S.A-1 to study the effect of non-symmetrical arrangement. Specimen S.A-2 has 10 tubes arranged in a symmetrical manner and closely packed inside the square tube. Specimen S.A-3 has 8 tubes arranged in a zig-zag manner that leave empty space inside the square tube. Nested stacked tubes arrangement is represented by specimen S.A-4. Table 2 shows the different parameters for each group.

Group 2 looks at the orientation of tubes; Ori-1, Ori-2 and Ori-3. Specimen Ori-1 has five tubes which are placed on top and perpendicular to each other. The tubes are positioned in the middle of each other. Specimen Ori-2 is similar to Ori-1 with the exception the tubes are positioned at the end of each other. Specimen Ori-3 consists of 5 layers of 2 tubes where each layer is oriented perpendicular to one another. Group 3 looks at the different thickness and diameter of tubes; S-1, S-2 and S-3. Specimen S-1 has 3 tubes with the same thickness but of different diameters i.e. 25 mm, 30 mm and 35 mm. Specimen S-2 has 3 tubes with the same diameter but of different thicknesses i.e. 0.5 mm, 1 mm and 1.5 mm. Specimen S-3 has 3 tubes with similar diameter and thickness. Dimension of specimen S-3 is the same as the fabricated specimen.

. Table 2: Groups of stacked tubes design (without the square tube)

Group 1	Group 2	Group 3
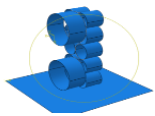 SA-1 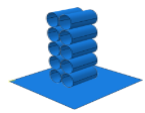 SA-2	 Ori-1	 S-1
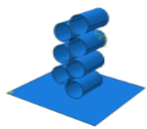 SA-3 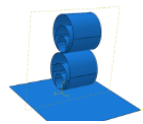 SA-4	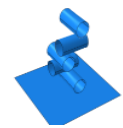 Ori-2	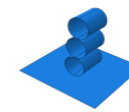 S-2
	 Ori-3	 S-3

Results and Discussions

Simulation validation

Figure 6 shows the simulation and experimental force-displacement curves of the baseline stacked tubes subjected to axial impact loading. Both showed high initial peak forces followed by lower mean forces. Simulation gave IPF of 42 *kN* while experiment recorded a value of 62 *kN*. Highly fluctuating curve from experiment was due to noise and vibration recorded by the sensors during impact. However, the simulation curve still showed good agreement with experiment in term of overall response of the stacked tubes. Simulation and experiment showed a difference of 32.2% in term of IPF. In experiment, a slight sideways movement of the circular tubes within the square tube during crushing resulted in IPF occurring at a slightly further distance compared to simulation.

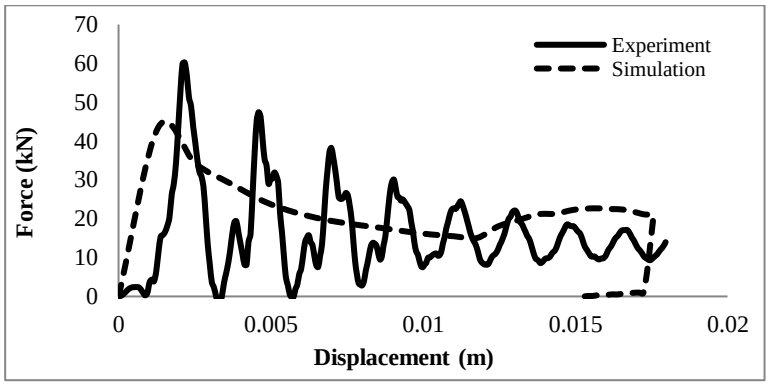

Figure 6: Simulation and experimental force-displacement curves of stacked tubes under axial impact loading

Collapse modes

Figure 7 shows the simulation and experimental final deformed shapes of the stacked tubes under axial impact loading. The different deformed shapes were due to several factors. In simulation, progressive buckling began at the bottom of the square tube with the bottom circular tube being crushed. The three circular tubes deformed in a consistent manner at their fixed positions. In experiment, due to the space between the circular tubes and the inner side wall of the square tube, upon impact, the circular tubes moved sideways before deforming. Buckling initiated at the middle of the square tube followed by lateral compression of the bottom circular tube. It is the combination of axial crushing of the square tube and lateral crushing of the circular tubes that give good impact energy absorption.

(a) 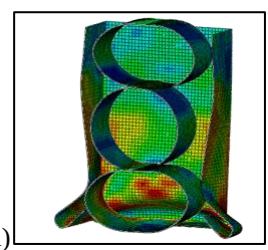 (b) 

Figure 7: Cross-sectional view of stacked tubes deformation under axial impact loading; (a) simulation (b) experiment

Comparison of crush performance indices for all configurations under axial static and impact loading

This section discusses the comparison of IPF, CFE, SEA and DAF between quasi-static and impact loading for all stacked tubes configuration. Results for axial static loading were obtained from previous work. Figure 8 shows the simulation force-displacement curves for all designs under axial impact loading. Most designs gave IPF values of 40 kN to 48 kN except for specimen S-3. It has the lowest IPF of 27 kN and longest crushing distance of 39 mm to ensure sufficient energy absorption. Final deformed shapes for all designs subjected to axial impact is shown in Figure 9. Due to springback of the circular tubes, there was a slight rebound of the impactor at the end of the crushing distance. These can be seen from the undeformed tubes in Figure 9.

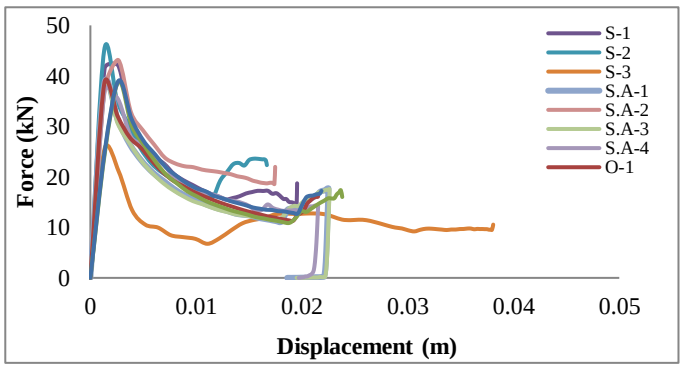

Figure 8: Simulation force-displacement curves of all stacked designs under axial impact loading

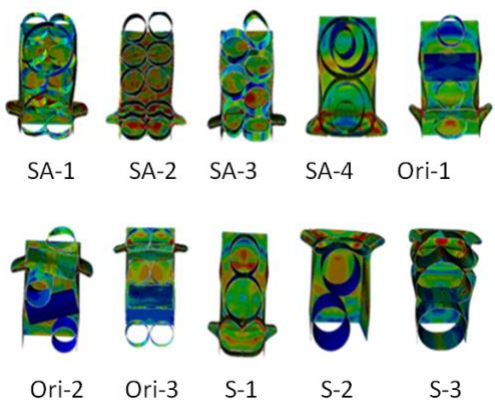

Figure 9: Final deformed shape of all designs when subjected to axial impact loading.

Figure 10 shows the IPF for all configurations subjected to axial static and impact loadings. IPF under impact loading were slightly higher compared to static loading for all configurations except for specimen S.A-4. The higher IPF was due to inertia effect. For specimen S.A-4, the large space between concentric rings within the square tube could contribute to lower impact IPF. For impact loading, specimen S-2 gave the highest IPF while specimen S-3 gave the lowest. It can be concluded that thickness and diameter of the circular rings have prominent effect on the IPF.

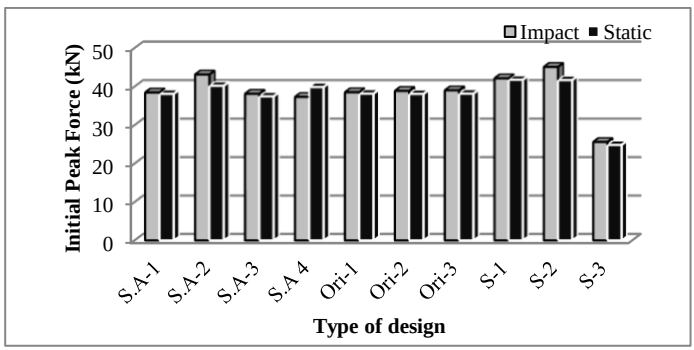

Figure 10: Comparison of IPF between different configurations under axial static and impact loadings

Figure 11 shows the CFE for all configurations subjected to axial static and impact loadings. CFE under static loading were higher compared to impact loading. This could be explained from the structure deformation. Figure 12 shows the final deformation of specimen S.A-2 under static and impact loading. Specimen under static loading has more plastic deformation at its top end compared to the specimen under impact loading. This plastic deformation resulted in higher mean force which increased the CFE. Also in static loading, deformation initiated at the top and propagated towards the bottom. For impact loading, due to stress wave propagation, deformation initiated at the weakest section of the specimen which was near the bottom end. Specimen S.A-2 has the highest CFE while specimen S-3 has the lowest.

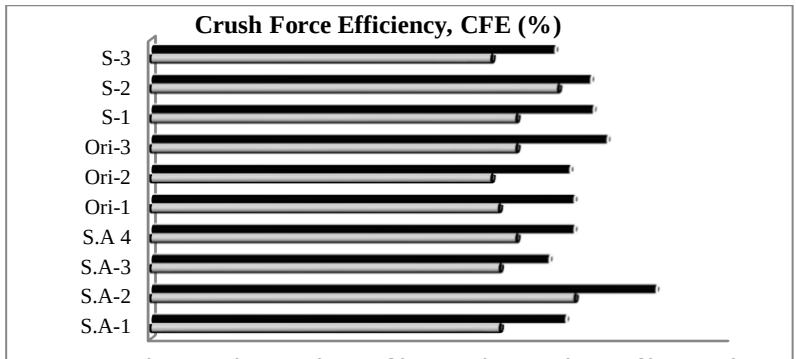

	S.A-1	S.A-2	S.A-3	S.A 4	Ori-1	Ori-2	Ori-3	S-1	S-2	S-3
Static	50	61	48	51	51	51	55	53	53	49
Impact	42	51	42	44	41.9	41	44	44	49	41

Figure 11: Comparison of CFE between different configurations under axial static and impact loadings

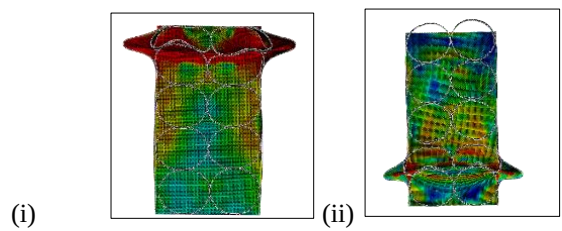

Figure 12: Specimen SA-2 after deformation under quasi-static (i) and impact loading (ii)

Figure 13 shows the SEA for all configurations subjected to axial static and impact loadings. Due to inertia effect, SEA under impact loading was higher compared to static loading for all configurations except for specimen S-3. Specimen Ori-1 has the highest SEA while specimen S.A-2 has the lowest. SEA is highly dependent on the failure mode since energy dissipation is by means of plastic deformation of the structure. Specimen Ori-1 has the highest SEA as it has high concentrations of plastic deformation. For specimen S-3, slightly lower SEA in impact as compared to static was due to the movement of the inner circular tubes during crushing. This resulted in less plastic deformation hence lowering the SEA.

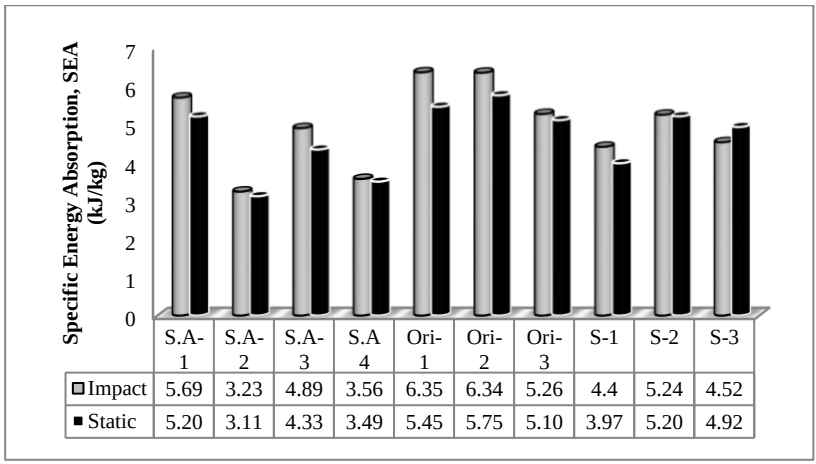

	S.A-1	S.A-2	S.A-3	S.A 4	Ori-1	Ori-2	Ori-3	S-1	S-2	S-3
Impact	5.69	3.23	4.89	3.56	6.35	6.34	5.26	4.4	5.24	4.52
Static	5.20	3.11	4.33	3.49	5.45	5.75	5.10	3.97	5.20	4.92

Figure 13: Comparison of SEA between different configurations under axial static and impact loading

Dynamic Amplification Factor (DAF) is the ratio of energy absorbed in impact loading to quasi-static loading. Figure 14 show the DAF for all configurations at equal crush distance. All configurations showed DAF values of 1 or more except for the S-3 design. This was due to the reason mentioned in the SEA. It is desirable to have DAF value of more than 1 as impact loading is more severe than static loading and therefore requires more energy absorption capability.

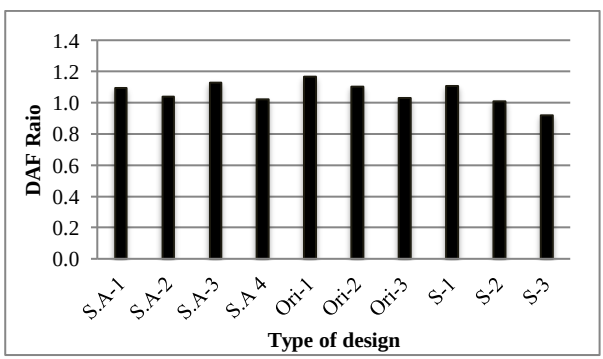

Figure 14: DAF for all configurations at equal crush distance

Figure 15 shows the acceleration-time curve for all configurations under axial impact loading. Acceleration values are usually compared to human injury criteria (HIC) in automotive design. Therefore it is important to quantify the value of maximum acceleration to ensure safety of the occupant. From the acceleration-time curves, all configurations showed high peak accelerations followed by decreasing acceleration with increasing time. Specimen S.A-2 has the highest peak acceleration while specimen S-3 has the lowest. Another important relationship to be quantified is the average G to peak G ratio. Figure 16 shows the ratio of average G to peak G for all configurations under axial impact loading. Specimen S-3 has the highest value while specimen S.A-1 has the lowest. The higher the value of average G to peak G, the safer will be the structure in absorbing the impact energy.

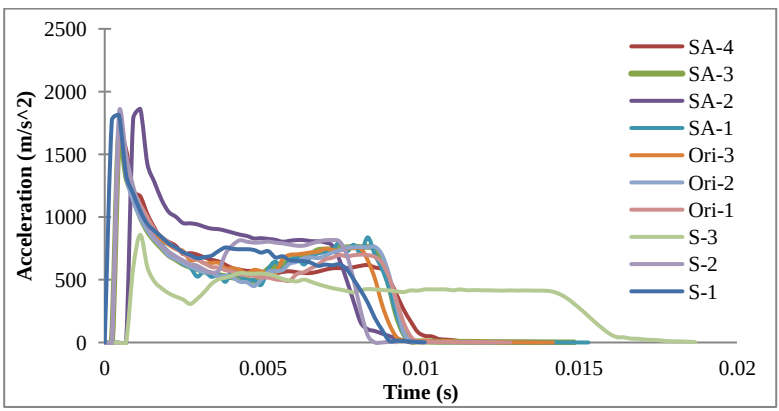

Figure 15: Acceleration-time curve for all configurations under axial impact loading

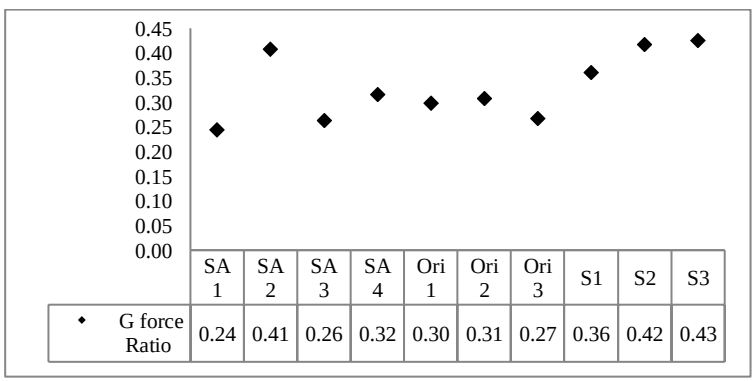

Figure 16: Ratio of average G to peak G for all configurations under axial impact loading

Conclusions

Comparisons of IPF, CFE and SEA between all configurations for axial static and impact loading were quantified and discussed. Overall, structures under impact loading showed higher IPF, CFE and SEA compared to static loading. Specimen S3 gave the lowest IPF and peak G, and highest average G to peak G ratio. Specimen S.A-2 gave the highest CFE. Specimen Ori-1 gave the highest SEA and DAF. It can be concluded that the type of tube arrangement, tube orientation and tube thickness have significant effect on the crush performance of structures. Findings from this work will be used to design an impact attenuator for UiTM Formula SAE car.

Acknowledgement

Our thanks to the Ministry of Education (MOE) and Universiti Teknologi MARA for their support under the Fundamental Research Grant Scheme (600-RMI/FGRS 5/3 (11/2015)) which are gratefully acknowledged.

References

[1] "Global Status Report On Road Safety 2015," World Health Organization (WHO), Switzerland, (2015).
[2] A. A. Faieza And H. Shahul, "The Effect Of Crashworthiness Parameters For Vehicle Body," Vol. 8354, No. 4, Pp. 1–6, (2015).
[3] A. A.Alghamdi, A. K.El-Kalay, T. M.,Abu-Mansoufi, & M.Akyufit, Absorption Of Energy By Frusta. Journal Of Islamic Academy Of Sciences, 5, 14-20, (1992).
[4] X. W. Zhang, H. Su, And T. X. Yu, "Energy Absorption Of An Axially Crushed Square Tube With A Buckling Initiator," Int. J. Impact Eng., Vol. 36, No. 3, Pp. 402–417, (2009).
[5] J. Song, Y. Chen, And G. Lu, "Light-Weight Thin-Walled Structures With Patterned Windows Under Axial Crushing," Int. J. Mech. Sci., Vol. 66, Pp. 239–248, (2013).
[6] M. Abbasi, S. Reddy, A. Ghafari-Nazari, And M. Fard, "Thin-Walled Structures Multiobjective Crashworthiness Optimization Of Multi-Cornered Thin-Walled Sheet Metal Members," Thin Walled Struct., Vol. 89, Pp. 31–41 (2015).

[7] M. B. Azimi And M. Asgari, "A New Bi-Tubular Conical-Circular Structure For Improving Crushing Behavior Under Axial And Oblique Impacts," Int. J. Mech. Sci., Vol. 105, Pp. 253–265, (2016).
[8] A. Jusuf, T. Dirgantara, L. Gunawan, And I. S. Putra, "Crashworthiness Analysis Of Multi-Cell Prismatic Structures," Int. J. Impact Eng., Vol. 78, Pp. 34–50, (2015).
[9] E.F.Abdewi, , S. Sulaiman, , A.M.S.Hamouda, E.Mahdi, , "Quasi-Static Axial And Lateral Crushing Of Radial Corrugated Composite Tubes," Thin-Walled Structures Vol 46, 320-332 (2008).
[10] X. Zhang, G. Cheng, Z. You, And H. Zhang, "Energy Absorption Of Axially Compressed Thin-Walled Square Tubes With Patterns," Thin-Walled Struct., Vol. 45, No. 9, Pp. 737–746, (2007).
[11] T. Jost, T. Heubrandtner, C. Ruff, And B. Fellner, "A New Method To Model Aluminium Honeycomb Based Crash Barriers In Lateral And Frontal Crash Load Cases," Pp. 13–24, (2008).
[12] M.A. Yahaya, D. Ruan, G. Lu And M.S. Dargusch, "Response Of Aluminium Honeycomb Sandwich Panels Subjected To Foam Projectile Impact – An Experimental Study," Int. J. Impact Eng., Vol 75, Pp. 100-109, (2015).
[13] H.Jonathan, K.Craig, L.Todd, P.Justin, "FSAE Impact Attenuator". Mechanical Engineering Department, 2010.
[14] G. Nagel, "Impact And Energy Absorption Of Straight And Tapered Rectangular Tubes," February, (2005).
[15] M. Raghupathi, M. Saravanan, and G. Sivakumar, "Comparison Of Crash Worthiness Of Two Materials Used In Bus Skeletal Frame," Vol. 2, No. 2, Pp. 22–30, (2015).